Invited Paper

Momentum-space Landau levels in arrays of coupled ring resonators

Hannah M. Price[a], Andrei C. Berceanu[b], Tomoki Ozawa[a], and Iacopo Carusotto[a]

[a]INO-CNR BEC Center and Dipartimento di Fisica, Università di Trento, I-38123 Povo, Italy
[b]Departamento de Física Teórica de la Materia Condensada & Condensed Matter Physics Center (IFIMAC), Universidad Autónoma de Madrid, Madrid 28049, Spain

ABSTRACT

Artificial magnetic fields for photons can significantly enrich the physics of coupled ring resonator arrays. We push this further to discuss how, under the addition of a harmonic potential, the photonic eigenstates can be recognised as novel Landau levels in momentum space.[1] We present two realistic experimental proposals in which this physics could be realised. Firstly, we discuss how to extend the experiment of Hafezi et al.,[2] where the artificial magnetic field was created using link resonators in a 2D ring resonator array. Secondly, we expand on a proposal in which an effective 2D photonic lattice is realised in a 1D ring resonator chain by exploiting a synthetic dimension for photons.[3] We show that momentum-space Landau levels would have clear signatures in spectroscopic measurements in such experiments, and we discuss the insights gained in this way into geometrical energy bands and particles in magnetic fields.[4]

Keywords: coupled ring resonators, synthetic gauge fields, topological energy bands, Berry curvature, magnetic eigenstates, synthetic dimension

1. INTRODUCTION

In recent years, there has been great progress in engineering artificial magnetic fields for neutral particles such as photons[5] and ultracold atoms.[6–8] These advances have been spurred on by the possibility of realising topological phases of matter, such as the integer or fractional quantum Hall effects, outside of traditional solid-state materials. Photonics experiments in resonator arrays, in particular, offer a high degree of controllability and tunability, as well as unprecedented experimental access to eigenstates and the eigenspectrum.[9] This was recently demonstrated by Hafezi et al.[2] who imaged the novel edge modes associated with the topological energy bands of a 2D ring resonator array in the presence of an artificial magnetic field.

Topological characteristics of these energy bands are also directly related to important geometrical properties such as the Berry curvature defined below.[10,11] Under an external force, the Berry curvature leads to a measurable drift of a semiclassical atomic wavepacket in an optical lattice[12–18] or a displacement of the photon distribution in a cavity array.[3,19] Remarkably, this can be understood as the Berry curvature acting on the atoms or photons as if it were a momentum-space magnetic field.[1,20–25] Replacing the external force by a weak harmonic trap, the analogy with magnetism becomes even more powerful as there is a direct correspondence between the effective momentum-space Hamiltonian of such a system and that of a charged particle in an electromagnetic field, except with the roles of position and momentum reversed. In special limits, the eigenstates of trapped particles in geometrically-nontrivial energy bands can therefore be understood as analogue magnetic states in momentum-space.[1,23–25] In particular, as we focus on here, when the energy band is approximately flat, these eigenstates are toroidal momentum-space Landau levels.[1,4] The observation of such states would represent the first investigation both of analogue magnetism in momentum space, as well as of magnetic states on a torus.

Photonics experiments in coupled cavity arrays offer an excellent opportunity to study momentum-space Landau levels. Firstly, as introduced above, artificial magnetic fields have already been experimentally realised in a 2D ring resonator array by introducing off-resonant link resonators.[2] As we have recently proposed[4] and as we detail here, a harmonic trap could be included in such a set-up via, for example, a spatial modulation of the resonator size. Secondly, we build on a recent proposal[3] that brings the powerful concept of a "synthetic dimension", originally introduced for ultracold atoms,[26–29] into integrated photonics. In this approach, the

Advances in Photonics of Quantum Computing, Memory, and Communication IX, edited by Zameer Ul Hasan, Philip R. Hemmer, Hwang Lee, Alan L. Migdall, Proc. of SPIE Vol. 9762, 97620W
 · doi: 10.1117/12.2218615

different modes of each ring resonator act as lattice sites along an additional dimension. With a suitable time-modulation of the resonator properties, these modes can be linearly coupled, so that photons are able to "hop" along this synthetic dimension, just as they can tunnel between different optical resonators. In this way, a 1D chain of resonators can behave like an effective 2D lattice. Furthermore, an artificial magnetic field can be straightforwardly introduced by means of a site-dependent inter-mode coupling amplitude.[3] Here, we show that this formalism can be further extended to include an external harmonic trapping potential, and so also to study momentum-space Landau levels.

Under a coherent pump, such experiments will be able to spectroscopically probe the eigenstates and eigenspectrum.[9] As we previously studied[4] and expand upon here, spectroscopic measurements should be able to observe key features of momentum-space Landau levels in systems with realistic experimental parameters. The inherent driving and dissipation present in these systems also provides access to new features such as inter-band geometrical properties and momentum-space cyclotron orbits. As the photon response depends an overlap between the eigenstates and the spatial profile of the pump, spectroscopic measurements will also be able to probe the specific artificial magnetic gauge implemented in a given experiment.[4]

The outline of this proceedings is as follows: we begin in Sec. 2 by introducing the 2D trapped Harper-Hofstadter (HH) model: an experimentally-relevant lattice model with eigenstates that are well-described as momentum-space Landau levels in particular parameter regimes.[1] In Sec. 3, we expand on our recent proposal[4] to explore this physics in a 2D ring resonator array by including link resonators and a harmonic trap. In Sec. 4, we propose an alternative approach that combines a harmonic trap with an effective 2D system, consisting of a 1D resonator chain with a synthetic dimension.[3] Finally, we present our conclusions in Sec. 5.

2. TOROIDAL LANDAU LEVELS IN MOMENTUM SPACE

As introduced above, we consider a harmonically-trapped particle in a geometrically-nontrivial energy band. Such energy bands arise in various contexts, such as for particles in (artificial) magnetic fields.[10] A simple and experimentally-relevant lattice model with nontrivial geometrical energy bands is the so-called Harper-Hofstadter Hamiltonian, defined below, describing a particle hopping on a tight-binding square lattice in the presence of a uniform magnetic field. As we now review, the eigenstates of this model, when combined with an external harmonic trap, can be understood as momentum-space Landau levels in certain parameter limits.

The full Hamiltonian describing the HH model $\mathcal{H}_0$ in the presence of an external harmonic trap is:

$$\mathcal{H} = \mathcal{H}_0 + \frac{1}{2}\kappa \sum_{m,n} \left[m^2 + n^2\right] \hat{a}^\dagger_{m,n}\hat{a}_{m,n}, \tag{1}$$

$$\mathcal{H}_0 = -J \sum_{m,n} (e^{i\phi^x_{m,n}} \hat{a}^\dagger_{m+1,n}\hat{a}_{m,n} + e^{i\phi^y_{m,n}} \hat{a}^\dagger_{m,n+1}\hat{a}_{m,n}) + \text{h.c.}, \tag{2}$$

where the operator $\hat{a}^\dagger_{m,n}$ creates a particle on a square lattice at site (m, n), κ is the harmonic trapping strength and $\hbar = e = 1$ throughout. Here, J is the real hopping amplitude, while $\phi = (\phi^x_{m,n}, \phi^y_{m,n})$ correspond to the Peierls phases gained by a charged particle hopping in a magnetic field.[30,31] For neutral particles, such as photons, these phases can be imposed artificially, as discussed below.

The total Peierls phase accumulated around a plaquette is given by $2\pi\alpha$, where α is the number of magnetic flux quanta per plaquette. However, the exact form of ϕ, and hence the phase of the eigenstates, is determined by the choice of magnetic gauge. The magnetic gauge enters into the phase of the eigenstates which usually is not an observable. However, in a photonics set-up, the intensity response depends on the overlap between the spatial amplitude profile of the pump and the eigenfunctions, and so, interestingly, experimental results can depend on the specific synthetic magnetic gauge implemented in an experiment.[4] For the purposes of this paper, we confine ourselves to the Landau gauge where $\phi = (0, 2\pi\alpha m)$.

The presence of the Peierls phases in $\mathcal{H}_0$ break the translational symmetry of the square lattice, unless a larger so-called magnetic unit cell is defined, containing an integer number of magnetic flux quanta.[13,32,33] We focus on values of the magnetic flux where $\alpha = 1/q$, with q being an integer, and choose the magnetic unit cell as q plaquettes along the x direction. The corresponding magnetic Brillouin zone (MBZ) is then smaller than

the original Brillouin zone (BZ) by a factor of q along the p_x direction. Within this new MBZ, the eigenstates of the HH model satisfy $\mathcal{H}_0|\chi_{n,\mathbf{p}}\rangle = E_n(\mathbf{p})|\chi_{n,\mathbf{p}}\rangle$, where $E_n(\mathbf{p})$ is the dispersion of the n-th energy band and $\mathbf{p}$ is the quasi-momentum in the magnetic Brillouin zone. The eigenstates themselves can be decomposed as $|\chi_{n,\mathbf{p}}\rangle = \frac{1}{\sqrt{N}} e^{i\mathbf{p}\cdot\mathbf{r}}|u_{n,\mathbf{p}}\rangle$, where N is the number of lattice sites and $|u_{n,\mathbf{p}}\rangle$ are the magnetic Bloch states.

The eigenstates of the full Hamiltonian $\mathcal{H}$ can then be expanded as $|\psi\rangle = \sum_n \sum_{\mathbf{p}} \psi_n(\mathbf{p})|\chi_{n,\mathbf{p}}\rangle$, where $\psi_n(\mathbf{p})$ are expansion coefficients. From the full Schrödinger equation $i\partial_t|\psi\rangle = \mathcal{H}|\psi\rangle$, it can be shown that:[1]

$$i\partial_t \psi_n(\mathbf{p}) = E_n(\mathbf{p}) + \frac{\kappa}{2} \sum_{n',n''} \left(\delta_{n,n'} i\nabla_{\mathbf{p}} + \mathcal{A}_{n,n'}(\mathbf{p})\right) \left(\delta_{n',n''} i\nabla_{\mathbf{p}} + \mathcal{A}_{n',n''}(\mathbf{p})\right) \psi_{n''}(\mathbf{p}), \tag{3}$$

where $\mathcal{A}_{n,n'}(\mathbf{p}) = i\langle u_{n,\mathbf{p}}|\nabla_{\mathbf{p}}|u_{n',\mathbf{p}}\rangle$ is the matrix-valued Berry connection: a geometrical property of the energy band. Provided that the harmonic trap is sufficiently weak compared to the energy band gap, we can make a single-band approximation, which assumes that only one coefficient ψ_n is non-negligible.[1] Then we arrive at $i\partial_t\psi_n(\mathbf{p}) = \widetilde{\mathcal{H}}\psi_n(\mathbf{p})$, where the effective momentum-space Hamiltonian is:[4]

$$\widetilde{\mathcal{H}} = \frac{\kappa}{2}[i\nabla_{\mathbf{p}} + \mathcal{A}_{n,n}(\mathbf{p})]^2 + \mathcal{E}_n(\mathbf{p}) \tag{4}$$

where we have grouped together terms in $\mathcal{E}_n(\mathbf{p}) = E_n(\mathbf{p}) + \frac{\kappa}{2}\sum_{n'\neq n} |\mathcal{A}_{n,n'}(\mathbf{p})|^2$. This momentum-space Hamiltonian is directly analogous to that of a charged particle in an electromagnetic field:

$$\mathcal{H}' = \frac{\left[-i\nabla_{\mathbf{r}} - \mathbf{A}(\mathbf{r})\right]^2}{2M} + \Phi(\mathbf{r}), \tag{5}$$

with the roles of position and momentum reversed. In this analogy, the particle mass M is replaced with κ^{-1}, the scalar potential $\Phi(\mathbf{r})$ by $\mathcal{E}_n(\mathbf{p})$, and the magnetic vector potential $\mathbf{A}(\mathbf{r})$ by the intra-band Berry connection $\mathcal{A}_{n,n}(\mathbf{p})$. In this analogy, the Berry curvature $\mathcal{F}_n(\mathbf{p}) = \nabla \times \mathcal{A}_{n,n}(\mathbf{p})$ acts like a momentum-space magnetic field $B(\mathbf{r})$. Remarkably, the topology of momentum space is also crucial here, as the MBZ is topologically equivalent to a torus. As we shall see below, this has various consequences, one of which is that, just as the magnetic field integrated over a torus is quantized according to the number of magnetic monopoles contained inside, so the Berry curvature over the whole MBZ is quantised in units of the first Chern number ν_n.[34]

In certain limits, the analogy with magnetism allows us to deduce the momentum-space eigenstates of Eq. 4 from the known real-space eigenstates of Eq. 5.[1,23,25] In particular, we consider here the flat-band limit of Eq. 4 in which the bandwidth of the lowest band is much smaller than the harmonic trapping strength. This approximation improves as either q or κ increase. In this case, we can approximate $\mathcal{F}_n(\mathbf{p}) \approx \mathcal{F}_n$ and $\mathcal{E}_n(\mathbf{p}) \approx \mathcal{E}_n$; then the first term in Eq. 4 is like the kinetic energy of a particle in a uniform magnetic field on a torus, while the second term is just a constant energy offset. The eigenstates of this effective Hamiltonian Eq. 5 are so-called toroidal Landau levels in momentum-space, with energies given by:

$$\epsilon_{n,\beta} = \mathcal{E}_n + \left(\beta + \frac{1}{2}\right)\kappa|\mathcal{F}_n|, \tag{6}$$

where the Landau level quantum number $\beta = 0, 1, 2, \ldots$, and where $\kappa|\mathcal{F}_n|$ is the analogue cyclotron frequency $\Omega_c = e|B|/M$. The degeneracy of these states equals the Chern number $|\nu_n|$, due to the toroidal topology of the MBZ. For odd values of q, $\nu_n = -1$ and $|\mathcal{F}_n| = q/2\pi$ in the flat-band limit for all bands except the middle band.[1] The toroidal topology of the MBZ also enters the analytical eigenstates, which for $\nu_n = -1$ are[1]

$$\chi_\beta(\mathbf{p}) = \left(\frac{\sqrt{2/q}}{2^\beta \beta! \times 2\pi l_{\mathcal{F}_n}^2}\right)^{1/2} \sum_{j=-\infty}^{\infty} e^{-ip_y j} e^{-(p_x + j l_{\mathcal{F}_n}^2)^2/2l_{\mathcal{F}_n}^2} H_\beta(p_x/l_{\mathcal{F}_n} + j l_{\mathcal{F}_n}), \tag{7}$$

where H_β are Hermite polynomials, $l_{\mathcal{F}_n} = \sqrt{1/|\mathcal{F}_n|}$ is the analogue magnetic length and where the phase of the Bloch states $|u_{n,\mathbf{p}}\rangle$ is chosen in such a way that the intra-band Berry connection $\mathcal{A}_{n,n}(\mathbf{p})$ is in the Landau-like gauge $\mathcal{A}_{n,n}(\mathbf{p}) = (0, \mathcal{F}_n p_x)$.

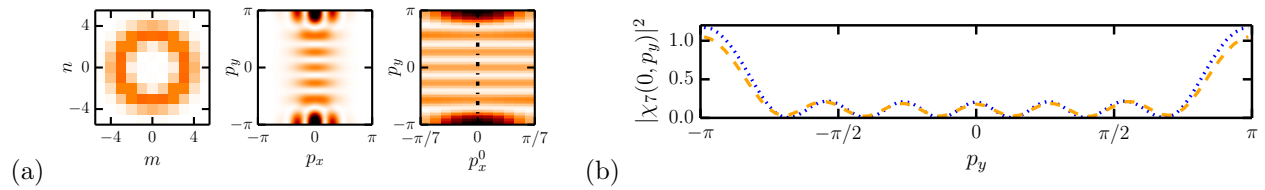

Figure 1. (a) The numerical 7th eigenstate of the full Hamiltonian (Eq.1) in real space (left), in momentum space (center) and the numerical population over bands in the MBZ (right) for $\kappa = 0.2J$ and $\alpha = 1/7$ in a small lattice of 11×11 sites. A cut along $p_x^0 = 0$ is indicated by a black dashed line. (b) The numerical population over bands for the cut along $p_x^0 = 0$ (dashed orange line) compared to the $\beta = 6$, $n = 0$ analytical Landau level (dotted blue line) from Eq. 7.

As previously shown,[1,4] these analytical results are in good agreement with numerics diagonalising the full Hamiltonian (Eq.1). As a reference for what follows in this work, we give an example in Figure 1 of the 7th eigenstate of a small lattice of 11×11 sites, with $\kappa = 0.2J$ and $\alpha = 1/7$. Numerically, the eigenstates of Eq. 1 were directly obtained in real space, and then Fourier-transformed into the original BZ. To reach the population over bands in the MBZ, a further transformation is required according to:[1]

$$\sum_n |\psi_n(\mathbf{p}_{\mathrm{MBZ}})|^2 = \sum_j |\psi(\mathbf{p}_{\mathrm{BZ}} = \mathbf{p}_{\mathrm{MBZ}} - j\mathbf{G})|^2, \tag{8}$$

where $\psi_n(\mathbf{p}_{\mathrm{MBZ}})$ is the coefficient in the MBZ and $\psi(\mathbf{p}_{\mathrm{BZ}})$ that in the full BZ. Here, j is an integer and $\mathbf{G} = (2\pi/q)\hat{\mathbf{p}}_x$ is the magnetic reciprocal lattice vector. Hereafter, we use $\mathbf{p}$ for the momentum in the full BZ, and $\mathbf{p}^0$ for that in the MBZ. As shown in Fig. 1(b), there is good agreement between the numerical population over bands and the analytical momentum-space Landau level, showing that our single-band approximation is reasonable; this agreement can be further improved by reducing κ to limit inter-band mixing.

3. MOMENTUM-SPACE LANDAU LEVELS IN A 2D CAVITY ARRAY

In a 2D array of ring resonators, photons can evanescently tunnel between resonators thanks to the spatial overlap of optical modes between neighbouring cavities. This leads to a tight-binding hopping Hamiltonian with a tunnelling amplitude J that decreases rapidly with the inter-resonator distance. Hopping phases, such as those in Eq. 2, can be introduced by letting the tunneling be mediated by additional off-resonant link resonators, as recently demonstrated experimentally[2] and as sketched in Figure 2(a). By displacing the link resonator between sites (m, n) and $(m, n+1)$ by an amount x_m, light gains a net phase-shift when circulating around a plaquette equal to[2] $\alpha = 4\pi n_{\mathrm{eff}}\,\Delta x/\lambda$, where $\Delta x = x_{m+1} - x_m$, n_{eff} is effective refractive index of the cavity material and λ is the wavelength of the light. Light circulating around the plaquette in the opposite direction experiences an opposite phase-shift $-\alpha$. Such an array therefore corresponds to two copies of the HH model, one for each

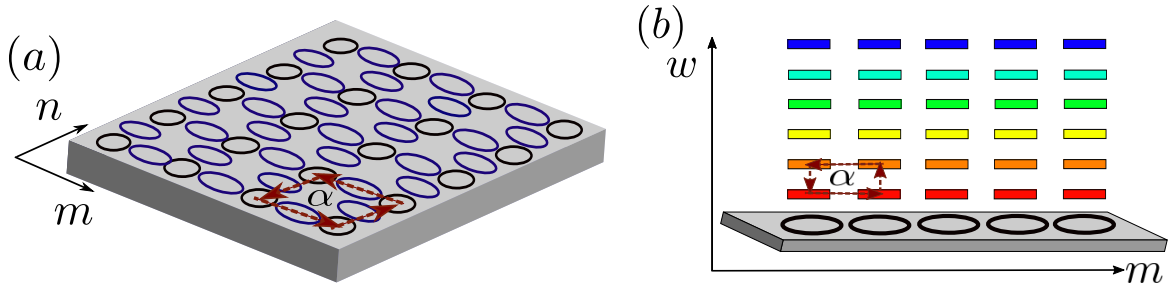

Figure 2. (a) A 2D array of cavities in which off-resonant microrings (in blue) are used to imprint an artificial magnetic flux α per plaquette on photons hopping between the resonant site microrings (in black).[2] (b) A 1D chain of resonators with a synthetic dimension provided by the different whispering gallery modes of each ring (indicated as coloured levels), creating an effective 2D lattice. Suitable design of the inter-mode coupling imprints a phase α on photons tunneling around the highlighted plaquette.

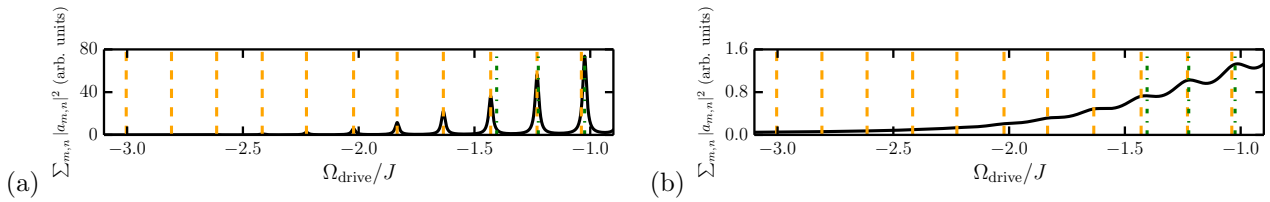

Figure 3. Intensity spectra for a small lattice of 11×11 sites with $\kappa = 0.2J$, $\alpha = 1/7$ and (a) $\gamma = 0.01J$ and (b) $\gamma = 0.1J$. The pump is situated at site $(5, 0)$. The first $n = 0$ (second $n = 1$) ladder of eigenstates from Eq. 1 is shown as orange (green) vertical dashed lines.

clockwise and another for each counter-clockwise whispering gallery mode of the ring resonator. Provided that backscattering coupling different modes can be neglected,[2] we can restrict ourselves to a single whispering gallery mode, realising Eq. 2. The harmonic trap can then be included by allowing the site resonator size to vary in space.[4]

While we have focused on conservative dynamics up to this point, an array of cavities is inherently a driven-dissipative system. Light continuously leaks out of the cavities, as we model theoretically by a uniform loss-rate γ. To balance these losses, light is also pumped into the system; we assume the pump is monochromatic, with frequency $\Omega_{\rm drive}$ and a spatial profile $f_{m,n}$. For non-interacting photons, the expectation value of the cavity field $a_{m,n}(t) \equiv \langle \hat{a}_{m,n}(t) \rangle$ evolves in the steady state as $a_{m,n}(t) = a_{m,n} e^{-i\Omega_{\rm drive} t}$ with amplitudes $a_{m,n}$ satisfying:

$$f_{m,n} = J\left[a_{m+1,n} + a_{m-1,n} + e^{-2i\pi\alpha m} a_{m,n+1} + e^{2i\pi\alpha m} a_{m,n-1}\right] + \left[\Omega_{\rm drive} + i\gamma - \frac{1}{2}\kappa\left(m^2 + n^2\right)\right] a_{m,n}. \quad (9)$$

This set of linear coupled equations can be solved numerically as a function of the pump frequency $\Omega_{\rm drive}$ to find $|a_{m,n}|^2$, the number of photons at each site (m, n), and the intensity spectrum $\sum_{m,n} |a_{m,n}|^2$, in which the different eigenmodes of the system appear as resonance peaks.[9] When the system is pumped on resonance with a state and losses are weak enough for this state to be spectrally separated by its neighbours, the near-field (far-field) spatial emission of photons reflects the real-space (momentum-space) wave function of that mode. The photon population over bands in the MBZ can also be found by processing the far-field emission according to Eq. 8. As we have recently demonstrated and as we show further here, key characteristics of momentum-space Landau levels may be observed in a 2D cavity array for realistic experimental parameters, such as a small lattice of only 11×11 sites with $\kappa = 0.2J$ and $\alpha = 1/7$.[4] We also restrict ourselves to $f_{m,n} = \delta_{m,m'}\delta_{n,n'}$, describing a pump at a singe site (m', n'), which models the injection of light into a single resonator at the system edge via an external integrated waveguide.[2]

In the absorption/transmission spectrum of the cavity array, toroidal Landau levels appear as equally-spaced peaks as shown in Figure 3 for (a) $\gamma = 0.01J$ and (b) $\gamma = 0.1J$. A high loss-rate broadens the resonance peaks, and so ideally experimental losses should be as small as possible. However, even for strong losses of $\gamma = 0.1J$, some peak positions can be distinguished. By measuring the overall position of these peaks, a cavity array experiment would also be able to extract the offset $\mathcal{E}_n$ and so measure inter-band geometrical properties in photonics for the first time.[4] We also note that the resonance-peak height increases with frequency $\Omega_{\rm drive}$; this is because the lowest momentum-space toroidal Landau levels are rings in real-space with radii that increase with frequency. As we pump a single site at the edge of the system, there is only substantial overlap between the pump and those eigenstates with radii comparable to the system size.[4] Other pumping schemes, although less easy to implement experimentally, can be used to excite different states and explore gauge-dependent physics.[4]

On resonance with a given mode, we observe that the spatial profile of the photons reproduces many features of the expected wave function. This is shown in Figure 4 for four different positions of the pumped single site. While there are distortions in the wave function due to the pumping and dissipation, many qualitative features remain such as the distinctive nodal positions. As the pumped site is moved, the photon distribution also changes significantly. The breaking of rotational symmetry arises from the interference of several Landau levels, due to the relatively large loss-rate. This can be understood as a cyclotron orbit in momentum space, providing a further demonstration of how the Berry curvature acts like a momentum-space magnetic field.[4]

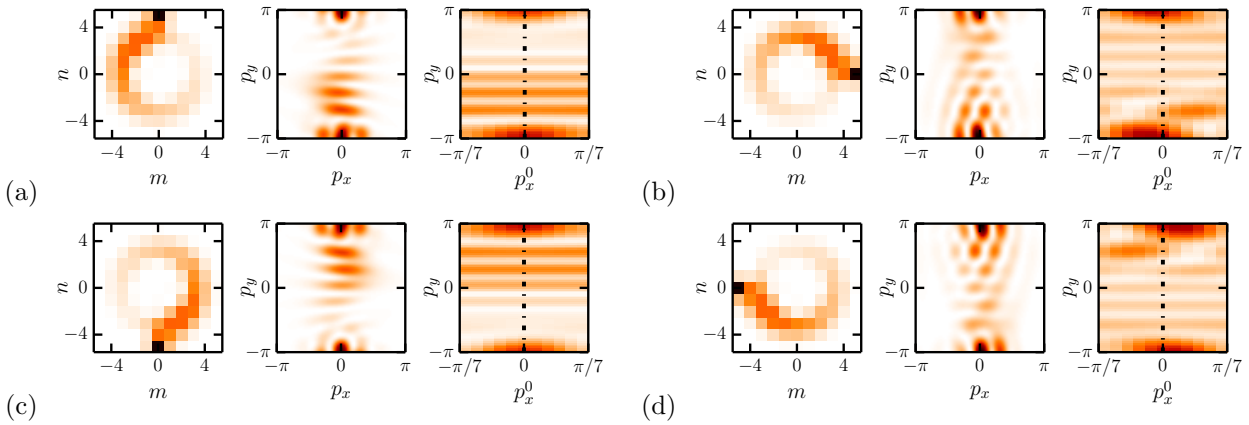

Figure 4. The photon intensity distribution found by numerically solving Eq. 14 for a single-site pump on resonance with the 7th eigenstate of the full Hamiltonian (1), for $\kappa = 0.2J$, $\gamma = 0.01J$ and $\alpha = 1/7$ in a small lattice of 11×11 sites. The pump is situated at site (a) $(0, 5)$, (b) $(5, 0)$, (c) $(0, -5)$ and (d) $(-5, 0)$. The photon distribution is shown in real space (left), in momentum space (center) and the MBZ (right).

4. MOMENTUM-SPACE LANDAU LEVELS IN A 1D RESONATOR CHAIN WITH A SYNTHETIC DIMENSION

As has recently been proposed,[3] another route towards realising a HH model (2) in a photonics set-up is to exploit the different whispering-gallery modes of each silicon ring resonator as an additional "synthetic" dimension. This approach can be used to explore an effective 2D lattice in a 1D chain of micro-rings as shown in Figure 2(b). Now we discuss how this formalism can be extended to include harmonic trapping and so also to realise toroidal Landau levels in momentum space.

The different resonance modes of a silicon ring can be labelled by an index w, which denotes the orbital angular momentum of each mode around the ring and which we now reinterpret as a lattice site index along a synthetic dimension. Photons can "hop" along this synthetic dimension provided that the different modes are coherently coupled. A suitable inter-mode coupling can be obtained by applying an external time-dependent modulation to the dielectric properties of each resonator[3] . Such a modulation could be induced, for example, via material nonlinearities under strong external light fields[3] or via electro-optic phase modulators.[35] It can be shown that the effective Hamiltonian for a 1D chain of resonators is then:

$$H = -\sum_{m,w} \left[\mathcal{J}_m(t)\, \hat{a}^\dagger_{m,w+\eta} \hat{a}_{m,w} + J \hat{a}^\dagger_{m+1,w} \hat{a}_{m,w} + \text{h.c.} + \Omega_{m,w} \hat{a}^\dagger_{m,w} \hat{a}_{m,w} \right] \tag{10}$$

where $\mathcal{J}_m(t)$ is the amplitude of the mode-coupling and $\Omega_{m,w}$ is the frequency (defined below) of mode w on a resonator with site index m along the chain. The hopping unit η is determined by the coupling mechanism between modes,[3] hereafter taken as $\eta = 1$. To arrive at a Hamiltonian like Eq.1, we would now like (i) to explicitly include a harmonic potential, (ii) to remove the time-dependence of $\mathcal{J}_m(t)$ and (iii) to simulate the hopping phases of the HH model.

An external harmonic potential can be included, as introduced above, by varying the ring radius R_m of the cavities spatially, such that the frequency of a reference mode w_0 at position (m) is $\Omega_{m,w_0} = \Omega_{0,w_0} + \frac{\kappa}{2} m^2$. Consequently, the mode frequency can be expressed as:

$$\Omega_{m,w} = \Omega_{0,w_0} + \frac{\kappa}{2} m^2 + \Delta\Omega_m \left(|w| - w_0 \right) + \frac{D_m}{2} (|w| - w_0)^2 \ldots, \tag{11}$$

where $\Delta\Omega_m = 2\pi c/(n_{\text{eff}} R_m)$ is the free-spectral range of ring (m) and D_m is the frequency dispersion due to the confinement geometry and to the residual refractive index dispersion of the material. For simplicity we assume hereafter that $D_m \approx D$. A crucial difference compared to the case with $\kappa = 0$ is that when we choose the modulation to be monochromatic $\mathcal{J}_m(t) = \mathcal{J}^o_m e^{-i\Omega_{\text{mod}} t}$, with a particular coupling frequency $\Omega_{\text{mod}} = \Delta\Omega_0$, there

will naturally be a spatially-dependent detuning away from $m = 0$. This can be seen by moving to a rotating frame by

$$\hat{b}_{m,w}(t) \equiv \hat{a}_{m,w}(t) e^{i[\Omega_{0,w_0} + (w-w_0)\Omega_{\rm mod}]t}, \tag{12}$$

where, focusing around $w \approx w_0$, we find the time-independent Hamiltonian:

$$\begin{aligned} H \;\approx\; & -\sum_{m,w} \left[\mathcal{J}^o_m \hat{b}^\dagger_{m,w+1} \hat{b}_{m,w} + J \hat{b}^\dagger_{m+1,w} \hat{b}_{m,w} + \text{h.c.} \right] \\ & + \sum_{m,w} \left[\Omega_{m,w_0} - \Omega_{0,w_0} + (\Delta\Omega_m - \Delta\Omega_0)(w - w_0) + \frac{D}{2}(w-w_0)^2 \right] \hat{b}^\dagger_{m,w} \hat{b}_{m,w}. \end{aligned}$$

As in a typical ring-resonator, a variation in the radius is reflected in a proportional shift of all mode frequencies and, in particular, of the free-spectral range $\Delta\Omega_m - \Delta\Omega_0 \approx w_0^{-1} (\Omega_{m,w_0} - \Omega_{0,w_0})$. We use this to arrive at:

$$H \approx \sum_{m,w} \left[-\mathcal{J}^o_m \hat{b}^\dagger_{m,w+1} \hat{b}_{m,w} - J \hat{b}^\dagger_{m+1,w} \hat{b}_{m,w} + \text{h.c.} + \left(\frac{\kappa}{2} m^2 + \frac{D}{2}(w-w_0)^2 + \frac{\kappa}{2w_0} m^2 (w - w_0) \right) \hat{b}^\dagger_{m,w} \hat{b}_{m,w} \right]. \tag{13}$$

This Hamiltonian contains both time-independent hopping terms as well as an effective harmonic trap along both the real spatial and the synthetic dimensions. The last term is an additional contribution stemming from the spatial dependence of the free-spectral range. As we shall see below, its effect is however negligible as soon as we are focusing on high-lying modes, $w_0 \gg 1$. Finally, to engineer the hopping phases of the HH model (2), we can engineer the modulation amplitude $\mathcal{J}^o_m$, for example, via the optical fields inducing this modulation through material nonlinearities.[3] Here, we choose the modulation to be $\mathcal{J}^o_m = |\mathcal{J}^o| e^{ik_x m}$, so that, as indicated in Figure 2(b), the hopping around a plaquette encloses an artificial "magnetic flux" $\alpha = k_x/2\pi$. Hereafter, we assume $|\mathcal{J}^o| = J$ and $D = \kappa$.

To model a driven-dissipative experiment, we can again include losses and pumping as in Sec. 3, except now with the field amplitudes $a_{m,n}(t) \equiv \langle \hat{a}_{m,n}(t) \rangle$ replaced by rotating-frame variables $\beta_{m,w}(t) \equiv \langle \hat{b}_{m,w}(t) \rangle$ to give

$$\begin{aligned} f_{m,w} \;=\; & J \left[\beta_{m+1,w} + \beta_{m-1,w} + e^{-2i\pi\alpha m} \beta_{m,w+1} + e^{2i\pi\alpha m} \beta_{m,w-1} \right] \\ & + \left[\Omega_{\rm drive} + i\gamma - \frac{1}{2}\kappa \left(m^2 + (w-w_0)^2 + \frac{1}{w_0} m^2 (w - w_0) \right) \right] \beta_{m,w}. \end{aligned} \tag{14}$$

We note that the single-site pump at (m', w') now has a frequency $\Omega_{m',w'} + \Omega_{\rm drive}$ in the non-rotating frame, where $\Omega_{\rm drive} \ll \Delta\Omega_{m'}$ ensures that only one mode is effectively driven.

The key difference now between this 1D cavity array and the 2D array in Sec. 3 is the appearance of the last term in Eq. 14. In Figure 5, we present numerical simulations for $w_0 = 6$ (left column) and $w_0 = 10$ (right column). In panels (a)&(b), we observe that the last term shifts the energies of the resonance peaks to the right as w_0 increases. In the limit of large w_0, where the last term in Eq. 14 can be neglected, we have checked that we obtain the spectrum previously found for a 2D array of cavities,[4] in which the peak positions are well-matched by the expected eigenstates of Eq. 1, shown here as orange (green) vertical dashed lines for the energy band $n = 0$ ($n = 1$). In panels (c)-(f), we also observe that the last term in Eq. 14 clearly affects the photon intensity distribution. For example, compared to a 2D array,[4] the photon distribution in the $m - w$ plane is distorted with respect to reflection around $w = w_0$, as the last term in Eq. (14) is sensitive to the sign of $(w - w_0)$. For increasing w_0, these effects are again rapidly suppressed. We have also checked that there is no qualitative change to this photon distribution as we move the pump frequency to the left to be exactly on resonance with the shifted peaks in panels (a)&(b).

Practically, experiments will focus around high-lying modes $w_0 \gg 1$, and so a 1D array with a synthetic dimension should be able to capture all the features of momentum-space Landau levels previously studied for the full 2D cavity array. We note, finally, that this set-up also has a key advantage that, due to the 1D geometry, any position (m', w') can be easily pumped via an external integrated waveguide, allowing a single experiment to access many more momentum-space Landau levels.

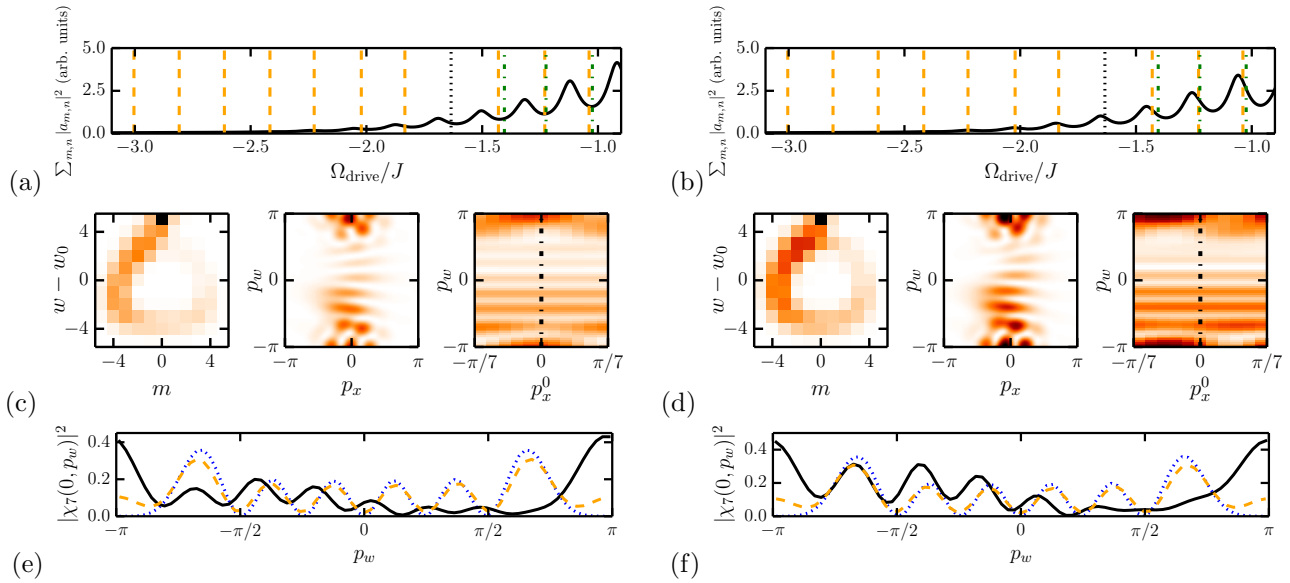

Figure 5. Numerical simulations of the photon steady state from Eq. 14 for a 1D resonator chain with a synthetic dimension, with $w_0 = 6$ (left column) and $w_0 = 10$ (right column), and $\kappa = 0.2J$, $\alpha = 1/7$ and $\gamma = 0.05J$ in a lattice of 11×11 sites, pumped at $(0, 5)$. (a)&(b) Intensity spectra showing for increasing w_0, the resonance peaks rapidly converge towards the expected eigenstates of Eq. 1, shown as orange (green) vertical dashed lines for the energy band $n = 0$ ($n = 1$). (c)&(d) The photon intensity distribution plotted in real space (left), momentum space (center) and the MBZ (right) filtered at the expected frequency of the 8th eigenstate of Eq. 1, as indicated in (a)&(b) by a black vertical dotted line. (e)&(f) The photon distribution for a cut along $p_x^0 = 0$ in the MBZ compared with the same cut for the conservative system (dashed orange line) and the $\beta = 7$ analytical toroidal Landau level (dotted blue line) from Eq. 7 with $n = 0$. The last term in Eq. 14 therefore appears to distort the wave function, without destroying the qualitative nodal structure. The agreement with previous results without the additional term[4] improves rapidly with increasing w_0.

5. CONCLUSIONS

In conclusion, we have discussed how momentum-space Landau levels could soon be observed experimentally in arrays of coupled ring resonators.[4] We have presented two distinct proposals for how to engineer these states by combining a harmonic trap with an artificial magnetic field for photons in, firstly, a 2D ring resonator array, and secondly, in a 1D resonator chain with a synthetic dimension. An observation of momentum-space Landau levels would be the first realisation of analogue magnetic states, as well as of magnetism on a toroidal surface.

We have also demonstrated that the main features of momentum-space Landau levels may be observed spectroscopically for systems with realistic experimental parameters. Furthermore, spectroscopic measurements will be able to access the absolute energy of eigenstates, measuring novel geometrical features of energy bands, such as a contribution from the inter-band Berry connection. The pumping and losses present in these experiments also open up the way towards studying analogue cyclotron orbits in momentum space and in exploring the role of the specific artificial magnetic gauge implemented in an experiment. Going further, it will be interesting in the future to explore the interplay of this physics with photon-photon interactions, to explore possible fractional quantum Hall states.[36,37]

ACKNOWLEDGMENTS

We are grateful to Ajit Srivastava, Ataç Imamoğlu and Germain Rousseaux for stimulating discussions. H.M.P., T.O. and I.C. were funded by ERC through the QGBE grant, by the EU-FET Proactive grant AQuS (Project No. 640800), and by Provincia Autonoma di Trento, partially through the project "On silicon chip quantum optics for quantum computing and secure communications - SiQuro". H.M.P was also supported by the EC through the H2020 Marie Sklodowska-Curie Action, Individual Fellowship Grant No: 656093 "SynOptic". A.C.B. acknowledges financial support from the ESF through the POLATOM grant 4914.

REFERENCES

[1] Price, H. M., Ozawa, T., and Carusotto, I., "Quantum mechanics with a momentum-space artificial magnetic field," *Phys. Rev. Lett.* **113**, 190403 (2014).

[2] Hafezi, M., Mittal, S., Fan, J., Migdall, A., and Taylor, J. M., "Imaging topological edge states in silicon photonics," *Nature Photon.* **7**(12), 1001–1005 (2013).

[3] Ozawa, T., Price, H. M., Goldman, N., Zilberberg, O., and Carusotto, I., "Synthetic dimensions in integrated photonics: From optical isolation to 4D quantum Hall physics," *ArXiv e-prints* , 1510.03910 (2015).

[4] Berceanu, A. C., Price, H. M., Ozawa, T., and Carusotto, I., "Momentum-space landau levels in driven-dissipative cavity arrays," *Phys. Rev. A* **93**, 013827 (2016).

[5] Hafezi, M., "Synthetic gauge fields with photons," *Int. J. Mod. Phys. B* **28**(02), 1441002 (2014).

[6] Dalibard, J., Gerbier, F., Juzeliūnas, G., and Öhberg, P., "*Colloquium* : Artificial gauge potentials for neutral atoms," *Rev. Mod. Phys.* **83**, 1523–1543 (2011).

[7] Goldman, N., Juzeliūnas, G., Öhberg, P., and Spielman, I. B., "Light-induced gauge fields for ultracold atoms," *Rep. Prog. Phys.* **77**(12), 126401 (2014).

[8] Goldman, N., Cooper, N., and Dalibard, J., "Preparing and probing Chern bands with cold atoms," *ArXiv e-prints* , 1507.07805 (2015).

[9] Carusotto, I. and Ciuti, C., "Quantum fluids of light," *Rev. Mod. Phys.* **85**, 299–366 (2013).

[10] Berry, M. V., "Quantal phase factors accompanying adiabatic changes," *Proc. R. Soc. London, Ser. A* **392**(1802), 45–57 (1984).

[11] Xiao, D., Chang, M.-C., and Niu, Q., "Berry phase effects on electronic properties," *Rev. Mod. Phys.* **82**, 1959–2007 (2010).

[12] Dudarev, A. M., Diener, R. B., Carusotto, I., and Niu, Q., "Spin-orbit coupling and berry phase with ultracold atoms in 2d optical lattices," *Phys. Rev. Lett.* **92**(15), 153005 (2004).

[13] Chang, M.-C. and Niu, Q., "Berry phase, hyperorbits, and the Hofstadter spectrum," *Phys. Rev. Lett.* **75**(7), 1348–1351 (1995).

[14] Price, H. M. and Cooper, N. R., "Mapping the berry curvature from semiclassical dynamics in optical lattices," *Phys. Rev. A* **85**, 033620 (2012).

[15] Cominotti, M. and Carusotto, I., "Berry curvature effects in the bloch oscillations of a quantum particle under a strong (synthetic) magnetic field," *Europhys. Lett.* **103**(1), 10001 (2013).

[16] Dauphin, A. and Goldman, N., "Extracting the chern number from the dynamics of a fermi gas: Implementing a quantum hall bar for cold atoms," *Phys. Rev. Lett.* **111**, 135302 (2013).

[17] Aidelsburger, M., Lohse, M., Schweizer, C., Atala, M., Barreiro, J. T., Nascimbene, S., Cooper, N., Bloch, I., and Goldman, N., "Measuring the chern number of hofstadter bands with ultracold bosonic atoms," *Nature Phys.* **11**(2), 162–166 (2015).

[18] Jotzu, G., Messer, M., Desbuquois, R., Lebrat, M., Uehlinger, T., Greif, D., and Esslinger, T., "Experimental realization of the topological haldane model with ultracold fermions," *Nature* **515**(7526), 237–240 (2014).

[19] Ozawa, T. and Carusotto, I., "Anomalous and quantum hall effects in lossy photonic lattices," *Phys. Rev. Lett.* **112**, 133902 (2014).

[20] Bliokh, K. and Bliokh, Y., "Spin gauge fields: From berry phase to topological spin transport and hall effects," *Ann. Phys.* **319**(1), 13–47 (2005).

[21] Wu, T. T. and Yang, C. N., "Concept of nonintegrable phase factors and global formulation of gauge fields," *Phys. Rev. D* **12**, 3845–3857 (1975).

[22] Cooper, N. R. and Moessner, R., "Designing topological bands in reciprocal space," *Phys. Rev. Lett.* **109**(21), 215302 (2012).

[23] Ozawa, T., Price, H. M., and Carusotto, I., "Momentum-space harper-hofstadter model," *Phys. Rev. A* **92**, 023609 (2015).

[24] Price, H. M., Ozawa, T., Cooper, N. R., and Carusotto, I., "Artificial magnetic fields in momentum space in spin-orbit-coupled systems," *Phys. Rev. A* **91**, 033606 (2015).

[25] Claassen, M., Lee, C. H., Thomale, R., Qi, X.-L., and Devereaux, T. P., "Position-momentum duality and fractional quantum hall effect in chern insulators," *Phys. Rev. Lett.* **114**, 236802 (2015).

[26] Boada, O., Celi, A., Latorre, J., and Lewenstein, M., "Quantum simulation of an extra dimension," *Physical review letters* **108**(13), 133001 (2012).

[27] Celi, A., Massignan, P., Ruseckas, J., Goldman, N., Spielman, I. B., Juzeliūnas, G., and Lewenstein, M., "Synthetic gauge fields in synthetic dimensions," *Phys. Rev. Lett.* **112**, 043001 (2014).

[28] Mancini, M., Pagano, G., Cappellini, G., Livi, L., Rider, M., Catani, J., Sias, C., Zoller, P., Inguscio, M., Dalmonte, M., and Fallani, L., "Observation of chiral edge states with neutral fermions in synthetic hall ribbons," *Science* **349**(6255), 1510–1513 (2015).

[29] Stuhl, B. K., Lu, H.-I., Aycock, L. M., Genkina, D., and Spielman, I. B., "Visualizing edge states with an atomic bose gas in the quantum hall regime," *Science* **349**(6255), 1514–1518 (2015).

[30] Harper, P. G., "Single band motion of conduction electrons in a uniform magnetic field," *Proc. Phys. Soc. A* **68**(10), 874–878 (1955).

[31] Hofstadter, D. R., "Energy levels and wave functions of bloch electrons in rational and irrational magnetic fields," *Phys. Rev. B* **14**, 2239–2249 (1976).

[32] Zak, J., "Magnetic translation group," *Phys. Rev.* **134**(6A), A1602–A1606 (1964).

[33] Zak, J., "Magnetic translation group. II. irreducible representations," *Phys. Rev.* **134**(6A), A1607–A1611 (1964).

[34] Fang, Z. et al., "The anomalous hall effect and magnetic monopoles in momentum space," *Science* **302**(5642), 92–95 (2003).

[35] Yuan, L., Shi, Y., and Fan, S., "Photonic gauge potential in a system with a synthetic frequency dimension," *ArXiv e-prints* , 1511.04612 (2015).

[36] Umucalılar, R. and Carusotto, I., "Fractional quantum hall states of photons in an array of dissipative coupled cavities," *Phys. Rev. Lett.* **108**(20), 206809 (2012).

[37] Hafezi, M., Lukin, M. D., and Taylor, J. M., "Non-equilibrium fractional quantum hall state of light," *New J. Phys.* **15**(6), 063001 (2013).